Near-isotropic enhancement of the 20 K critical current of $REBa_2Cu_3O_7$ coated conductors from columnar defects

OPEN ACCESS
IOP Publishing
Superconductor Science and Technology
Supercond. Sci. Technol. **36** (2023) 055001 (10pp)
https://doi.org/10.1088/1361-6668/acbac6

Near-isotropic enhancement of the 20 K critical current of $REBa_2Cu_3O_7$ coated conductors from columnar defects

Nicholas M Strickland[1,*], Stuart C Wimbush[1], Arya Ambadiyil Soman[1], Nicholas J Long[1], Martin W Rupich[2], Ruth Knibbe[3], Ming Li[3], Christian Notthoff[4] and Patrick Kluth[4]

[1] Robinson Research Institute, Victoria University of Wellington, Lower Hutt 5010, New Zealand
[2] American Superconductor Corporation, Ayer, MA 01432, United States of America
[3] School of Mechanical and Mining Engineering, University of Queensland, Brisbane, QLD 4072, Australia
[4] Research School of Physics, Australian National University, Canberra, ACT 2601, Australia

E-mail: nick.strickland@vuw.ac.nz

Received 27 September 2022, revised 31 January 2023
Accepted for publication 9 February 2023
Published 9 March 2023

Abstract

Normal-incidence irradiation by 100 MeV Ag ions is used to improve flux pinning in previously optimised commercial REBCO tapes from the American Superconductor Corporation. We observe distinct critical-current anisotropy enhancements below and above 40 K. Above 40 K a strong *c*-axis peak appears in the angular dependence of the critical current, as is usually expected upon the introduction of columnar defects. The critical current is enhanced significantly but only for a limited range of field angles. Close to the parallel-field direction there is no enhancement or even a reduction in critical current. Below 40 K, on the other hand, the enhancement is much broader with respect to field angle, creating an almost isotropic response at 20 K, 3 T. The absence of a prominent *c*-axis peak does not indicate a lack of pinning, since the absolute value of the critical current still increases by a factor of 2.8 compared to an unirradiated sample. Instead, we postulate that pre-existing point-like pinning centres act to mediate an interaction between the existing planar and newly-introduced columnar pins, broadening both contributions. The point-like pins become less effective with increasing temperature as the coherence length increases, leading to a reduction in this interaction and a separation of the individual peaks relating to planar and columnar pins. At 20 K, we achieve an enhancement in the angular-minimum critical current by a factor of 2.7, in a material that had already been process-optimised for low-temperature pinning.

Keywords: REBCO coated conductors, ion irradiation, columnar defects, critical current anisotropy, maximum entropy

(Some figures may appear in colour only in the online journal)

* Author to whom any correspondence should be addressed.

1. Introduction

$REBa_2Cu_3O_7$ (REBCO, where RE is a rare earth element) coated conductors are a mature high-temperature superconductor (HTS) technology, produced in commercial quantities by several manufacturers. The REBCO thick-film layer of the conductor can be deposited by several quite different deposition methods. For each of these deposition methods, there are various ways of deliberately introducing nano-scale defects, secondary phase inclusions or impurity phase particles [1–19]. Such variations typically take some development time to optimise, but are a convenient way to introduce additional flux pinning. The nature of the additional flux pinning—the range of temperatures, magnetic fields and magnetic-field angles over which it is enhanced—depends on the size, geometry and number-density distributions of the defects. In particular, the effect on critical current anisotropy—its dependence on magnetic field orientation—is largely influenced by the dimensionality, spatial distribution and average orientation of the defects. Elongated or linearly correlated particles [2–6] and planar defects [7–10] enhance flux pinning over a preferential range of field angles corresponding to magnetic fields being parallel to these structures, while spherical or randomly oriented particles [11–18] tend to provide flux pinning over a wide range of field orientations and mixed pinning landscapes can be created combining the benefits of both [19]. Another class of defects that is known to enhance flux pinning is that introduced by the passage of energetic ions through the REBCO film [20–36]. These can leave point-like or track-like defects ranging from single-atom displacements to disruption radii of several nanometres depending on the mass and energy of the ion species used. With appropriate selection of ion species and energy, such a process can be sufficiently rapid to be applied to a long-length tape in an industrial process [25, 37]. From a more academic viewpoint, the irradiation-induced defect size range is ideal for investigating the limits of flux pinning in REBCO since it is a good match for the *ab*-plane coherence length.

A particular advantage of ion-beam induced defects is that they are typically produced *ex-situ*, that is to say after the REBCO layer has been deposited, reacted and oxygenated and so do not substantially change the existing defects. In that sense, the defects can be considered to be perfectly additive with respect to the existing pinning landscape. This provides an opportunity to investigate cumulative pinning effects in some detail. At the same time, the added defect density can be well controlled through the ion fluence, and the defect size to a certain extent through the ion species and energy. Through these two parameters, one can optimise pinning for different regimes of magnetic field (through defect density/ion fluence) and temperature (through defect size/ion energy).

While the defects are additive, we do not expect the resultant pinning to be perfectly additive since different families of defects with different pinning characteristics can combine to either enhance or diminish pinning in quite different ways. For example, a set of parallel columnar defects in an otherwise clean sample will produce strong pinning only when the field is oriented parallel to those defects. With two such families of defects at different angles, pinning will be strong not only for those two different orientations, but also for intermediate orientations where vortices will form well pinned staircase-like configurations [29, 33]. Conversely, once the defect density becomes appreciable there is also an increasing likelihood of overlap of defects, which ultimately can reduce pinning in a super-linear fashion [11].

In this paper, we have investigated irradiation with 100 MeV Ag ions at normal incidence. At this energy, the induced defects are discontinuous columnar tracks [36]. These are well known to produce a highly anisotropic pinning enhancement at higher temperatures, around 77 K, but give modest overall enhancement as judged by the angular minimum critical current at those temperatures. Here, we confirm those results and further show that under similar conditions of irradiation energy and fluence a significant, and almost isotropic, enhancement by a factor of 2.7 of the angular minimum I_c can be achieved at 20 K.

2. Experimental methods

2.1. Samples

Samples were cut from a 1 cm-wide long-length tape manufactured by the American Superconductor Corporation (AMSC). The tape had a good uniformity of 77 K I_c determined from a magnetisation scan (better than 5% over the length of tape used in this study). They consist of a 1.5 μm thick film of Dy-doped $YBa_2Cu_3O_7$ with nominal composition $YBa_2Cu_3O_7$: $0.25Dy_2O_3$ grown by metal-organic deposition on a Ni: 5% W substrate textured by the RABiTS process [37]. The Dy_2O_3 tends to form nanoparticles within the REBCO matrix, although the Y and Dy interchange essentially completely. A silver cap layer was deposited on the REBCO; this layer was made thinner than usual, only 1 μm thick, to reduce its impact on the ion beam.

Samples were patterned by photolithography and wet etching to produce a current bridge 5 mm long and 0.5 mm wide to give a well-defined irradiation area. Uncertainty in the bridge width is less than 2%.

Irradiation with 100 MeV Ag ions was carried out at the Australian National University's Heavy Ion Accelerator Facility. Ion fluences of between 1×10^{11} cm^{-2} and 6×10^{11} cm^{-2} have been applied, corresponding to matching fields of between 2.1 T and 12.4 T (under the approximation of one pinning centre per ion track) with irradiation times of up to 2 min. The average ion energy diminishes as it passes through the silver cap layer and the HTS layer itself; from 100 MeV at the surface the energy reduces to 73 MeV at the top of the HTS layer to 50 MeV at the bottom [36]. The ion beam was rastered over a 6 mm $\times$ 3 mm area to provide a uniform coverage of the current bridge. Care was taken to irradiate slightly beyond the bridge region since in favourable cases the critical current could be significantly enhanced in the irradiated region, giving the possibility of burnout in the unirradiated region of the sample.

2.2. Post-irradiation annealing

All samples intended for transport measurements were annealed at a temperature of 250 °C in 1 atm flowing oxygen gas for 1 h after irradiation. This level of annealing has been found to improve both the transition temperature T_c and the critical current I_c measured in zero applied magnetic field through re-ordering of oxygen in the REBCO lattice but is not high enough to anneal out the ion damage tracks. We found that the I_c measured at all temperatures and fields was improved by this level of annealing, compared to the freshly irradiated materials.

Suppression of T_c following the combination of irradiation and post-annealing is approximately linearly dependent on irradiation fluence in the range investigated, with a 3 K reduction for the highest fluence tested of 6×10^{11} cm^{-2}.

2.3. Transmission-electron microscopy

Samples for microscopy were not annealed after irradiation. Sample cross sections were prepared with a FEI Scios focused ion beam system and images were taken with a Hitachi HF 5000 transmission electron microscope (TEM).

2.4. Critical current measurement

The critical current was measured over a range of temperatures, magnetic fields and magnetic field angles on a SuperCurrent four-probe transport measurement system [38]. Currents of up to 1200 A, sample temperatures below 15 K, magnetic fields up to 8 T and full angle dependences in the maximum Lorentz force configuration could be measured with this system.

3. Results

3.1. Microstructure

The passage of 100 MeV Ag ions through the sample creates linear damage tracks. In the crystalline REBCO layer these present as amorphised regions and are therefore readily observed by TEM (vertical columns in figure 1). At this energy the tracks form discontinuous columns [36]. The observed tracks have an average diameter of 3.0 ± 0.2 nm and discontinuous segment lengths of between 50 nm and 150 nm; however, the disordered nature of these films preclude a detailed statistical analysis of segment lengths. It has been argued that discontinuous columns are a preferred structure for flux pinning as they provide moderately strong pinning with less disruption to a transport current than continuous columns [33]. The planar defects (horizontal in figure 1) and isotropic nanoparticles evident are also present in the unirradiated samples and are part of the process-optimised pinning landscape in commercially available AMSC conductors.

3.2. Angle dependence of critical current

The angle dependences of the critical current $I_c(\theta)$ at temperatures between 77 K and 20 K (top to bottom) and at magnetic fields between 1.0 T and 8.0 T (left to right) are shown in figure 2. An unirradiated sample and samples irradiated at three fluences ranging up to 6×10^{11} cm^{-2} are shown.

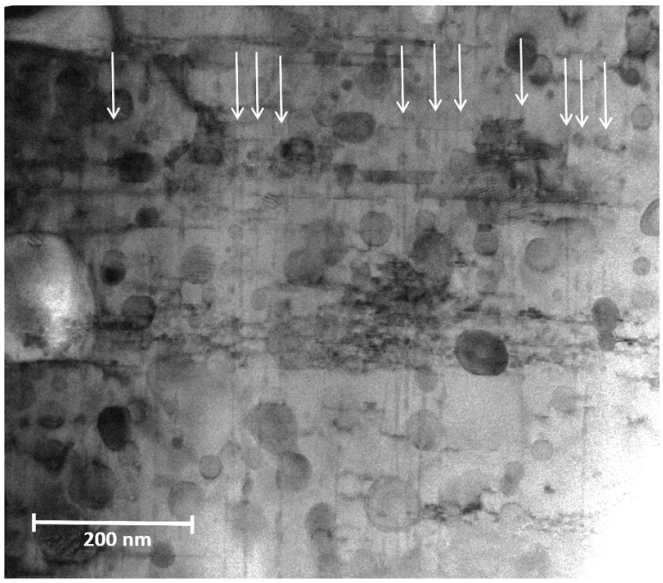

Figure 1. TEM cross-section image of the REBCO layer after irradiation with 100 MeV Ag ions to a fluence of 1×10^{11} cm^{-2}. Irradiation introduces discontinuous columnar tracks of amorphised REBCO. The tracks are approximately parallel to the REBCO *c*-axis and representative tracks are indicated by arrows. Planar (horizontal) features and nanoparticles are normal features of the unirradiated sample.

The unirradiated material as produced by AMSC is unusual in having an inverted *ab*-plane peak at 90° at 77 K and 1 T, where it is commonplace to instead observe a large peak at 90° under this condition [7]. The usual *ab*-plane peak arises at 77 K mainly as a result of Y124-type stacking faults, which form under high-temperature annealing conditions in an oxygen atmosphere, such as during oxygen-loading processes [8–10]. In this particular sample, the peak has been significantly suppressed by careful control of the annealing process. Non-extended pinning centres such as nanoparticles and point defects produce strong isotropic pinning, and the appearance of a dip, or inverted peak, at 90° actually occurs due to broad *c*-axis pinning centred at 0°. As the temperature is reduced, the inverted *ab* peak becomes a strong conventional peak as the dominant *ab* pinning mechanism switches from stacking faults at higher temperatures to intrinsic pinning at lower temperatures, with a threshold between 50 K and 65 K [39, 40].

At 77 K, irradiation at the fluences tested produces a large peak in the angle dependences centred at 0°, which is the expected result of columnar defects arising from a normal-incidence ion beam. At the same time though, there is a general reduction in zero-field I_c arising partly from the reduction in T_c and partly from reduced current percolation and this tends to give a reduction in I_c away from the peak. At 77.5 K, 3.0 T for example, a fluence of 1×10^{11} cm^{-2} produces a large 0° peak roughly doubling I_c at that angle, but slightly reduces I_c at 90°. The overall effect is to slightly improve the angular

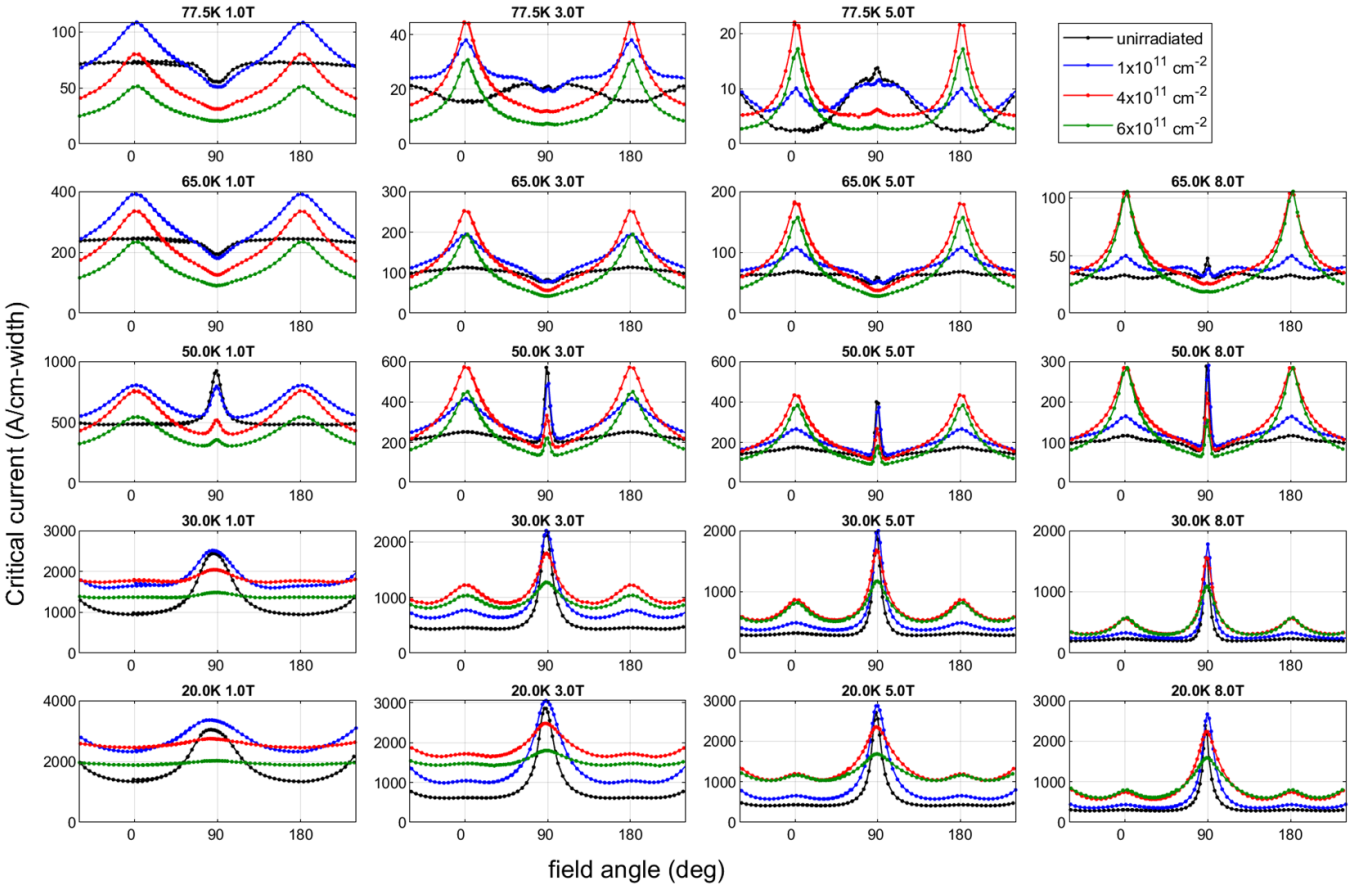

Figure 2. Angle dependence of the critical current of the sample before irradiation and following three increasing fluences of 100 MeV Ag irradiation. Plots are shown at five different temperatures (top to bottom) and at four different magnetic fields (left to right).

minimum I_c denoted I_c^{min} which is a useful metric for assessing the benefit or otherwise of anisotropic pinning modifications [41]. As the fluence is increased, the 0° peak increases but the 90° reduction is greater, leading to a reduced I_c^{min}.

The effect of irradiation on I_c^{min} as measured at moderate fields (3 T–5 T) does not become appreciably more beneficial as we measure at lower temperature until below 40 K. At 50 K, the sharp 90° peak associated with intrinsic pinning begins to emerge in all samples and the large peak arising from the irradiation columnar defects complements this. However, the angular region immediately adjacent to the 90° peak now has the lowest I_c point and after irradiation this I_c^{min} is still comparable to or lower than that of the pristine sample.

Below 40 K, the intermediate angle range between 0° and 90° begins to fill in and by 30 K it is clear that all fluences tested have an enhanced I_c^{min} relative to the unirradiated sample. At 30 K and 3 T a fluence of 4×10^{11} cm^{-2} provides the optimum enhancement, while in the range of 5 T–8 T 4×10^{11} cm^{-2} and 6×10^{11} cm^{-2} give a similar enhancement. Following this trend, it seems likely that even higher fluences would be required to optimise pinning at fields higher than 8 T. The presence of a field-dependent optimum fluence reflects the usual behaviour of pinning centres. A certain number of defects act to pin vortices; however, when more defects are present than are required to pin the vortices, this tends to promote flux creep, reducing I_c. Naturally, the higher the field, the higher the density of defects required to form the optimum pinning landscape. At 20 K, 3 T the irradiation produces a remarkably isotropic enhancement. The 0° peak evident in the unirradiated sample, and also in the irradiated samples at higher temperatures, becomes so broad as to be barely discernible and the angular minimum of I_c has been enhanced by a factor of 2.7. As the fluence increases, the *ab* peak diminishes as well, so the curve tends to become even more isotropic. At higher fields up to 8 T the 0° peak becomes more apparent, but is still relatively less conspicuous than at the higher temperatures.

This behaviour shows the necessity of measuring the angle-dependence of I_c, since a deep minimum can often occur at an intermediate angle. In figure 3(a) we show the temperature dependence of I_c for a 5 T perpendicular field and in figure 3(b) the equivalent I_c^{min}. Relying on perpendicular-field I_c we would see an I_c enhancement at all temperatures and across the full range of fluences tested here. At 50 K, for example, we have already a factor of 2.5 enhancement in perpendicular-field I_c. From the angle dependence though we can see that this enhancement is limited to the angular range close to perpendicular field, and the I_c^{min} values shown in figure 3(b) are similar to or even less than the unirradiated sample. While such

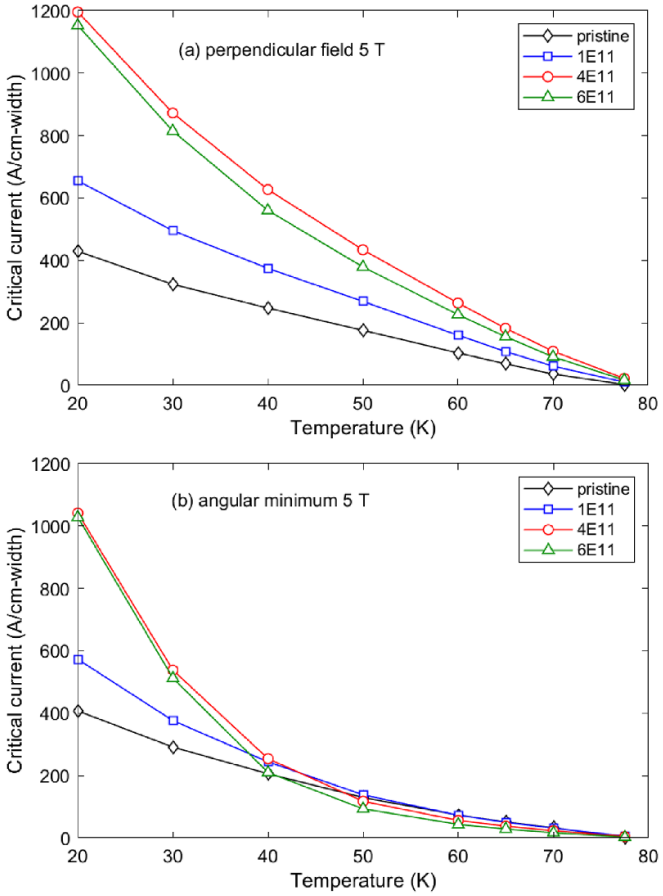

Figure 3. Temperature dependences of the critical current in a 5 T magnetic field for (a) perpendicular field, and (b) the angular minimum, for the unirradiated and 100 MeV Ag irradiated samples.

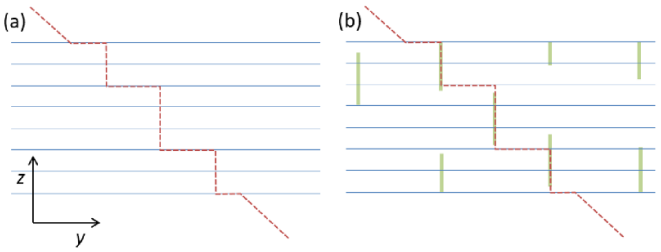

Figure 4. Schematic illustration of staircase vortices conforming to extended parallel defects. (a) With a single population of parallel defects (e.g. intrinsic pins) the inclined vortex can slide laterally along the parallel defects, leading to weak pinning. (b) With an additional population of orthogonal defects or isotropic defects the staircase vortex can be pinned, potentially with greater pinning force than from either defect population alone. The y–z axes refer to the discussion in section 3.3

enhancements over a limited range of angles could be beneficial for specific applications or magnet configurations, clearly the information is incomplete. It is not until below 40 K that irradiation becomes truly beneficial in terms of the I_c^{min} shown in figure 3(b). I_c then rises rapidly with decreasing temperature giving a 2.7-fold enhancement in I_c^{min} at 20 K.

We interpret this behaviour of an intermediate-angle 'valley' filling in at lower temperatures as reflecting the strength of flux pinning available to staircase vortices when the field is applied at intermediate angles. This is illustrated in figure 4. When only intrinsic planar pinning is available, inclined vortices form staircase vortices to maximise their overlap with the non-superconducting regions between the CuO_2 planes. However, the vertical sections of these vortices are unpinned leaving them free to slide laterally. In such a case, one would expect a very sharp peak in I_c at 90° when the field is in the *ab* plane, and any deviation from that angle would have low I_c. In the unirradiated samples of this study, there also exists a moderate density of nanoparticles and point defects that act to pin those vertical sections so the 'isotropic background' is raised to a useful practical level. This is evident from the angular dependences of figure 2 at 20 K and 3 T–8 T, which have a very flat background over a wide range of angles away from the 90° peak. When discontinuous columnar defects are added through ion irradiation, this adds a population of orthogonal complementary pinning centres, with a strong pinning component for the vertical sections of the vortex. The functional form of the I_c angular dependences then depends on the relative effectiveness and density of the different anisotropic and isotropic pinning populations.

Notably, the significant broadening of the 90° peak does not occur following proton irradiation [42], in which an increased density of point-like defects also gives a near-isotropic lift. This suggests that a three-way combination of planar, columnar and point-like pins is required to deliver the broadening effect on both 0° and 90° peaks. As we look to higher temperatures the isotropic contribution of point-like defects that occur naturally in all the samples, including unirradiated, reduces as the coherence length increases. This results in the 0° and 90° peaks becoming more distinct and by 50 K there are intermediate angles at which I_c is as low as, or lower than, that of the unirradiated sample.

3.3. Maximum entropy model

We can quantify these effects by using the maximum entropy vortex-path model [43–46]. In this model, the $I_c(\theta)$ function is fitted with a sum of angular Lorentzian and angular Gaussian functions, derived from a statistical analysis of vortex path choices with either Lorentzian or Gaussian statistics governing a meander path through the sample. Pinning of staircase vortices is central to this model, with combinations of pinning centres contributing to the variation of pinning strength with average field angle, as depicted in figure 4. Considering pinning to occur in the y–z plane of the sample, Gaussian distributions arise when a pinning strength distribution $f(y/z)$ has a statistically robust mean and variance, while Lorentzians arise from heavy-tailed distributions such as those with multiple pinning populations with different pinning strengths in either y or z directions. The angular-Gaussian or angular-Lorentzian distributions thus encode the information available at the macroscopic scale due to the averaging over the ensemble of all

microscopic states accessible by the system. The assignment of Lorentzian and Gaussian peak shapes to populations of defects is made based on our microstructural knowledge of the sample (through TEM and the known sample preparation such as irradiation dose), consistency with accepted vortex physics, and correlations between changes in structure and changes in the fitted I_c components. The analysis method is to proceed with fitting such that residuals are of the order of the noise level of the measurement and then assign peaks with defect populations in cases where there is sufficient evidence to make an assignment with reasonable confidence.

Angular Lorentzian peaks take the form

$$I_c(\theta) = \frac{I_0}{\pi\Gamma} \frac{1}{\cos^2(\theta-\theta_0) + \left({}^1\!/_\Gamma\right)^2 \sin^2(\theta-\theta_0)} \quad (1)$$

while angular Gaussian peaks take the form

$$I_c(\theta) = \frac{I_0}{\sqrt{2\pi}\Gamma} \frac{1}{\cos^2(\theta-\theta_0)} \exp\left(-\frac{\tan^2(\theta-\theta_0)}{2\Gamma^2}\right), \quad (2)$$

where I_0 and Γ are intensity and peak-shape parameters, respectively, for peaks centred at $\theta = \theta_0$ and here we have defined the Lorentzian functions such that for $\Gamma < 1$ larger Γ gives broader features with $\Gamma = 1$ giving a purely isotropic contribution. The Gaussian form gives a double-peak bifurcated shape when $\Gamma > 1/\sqrt{2}$.

The decomposition of the I_c anisotropy into maximum entropy functions are shown in figure 5 for the unirradiated sample and the three irradiated samples. Each is shown at 20 K, 5 T and 50 K, 5 T. The assignment of components to the main microstructural features determining the distribution means is summarised in table 1. In each case, it is the combination with other defects that give rise to the distribution variance (broadening).

The unirradiated sample at 20 K, 5 T can be fitted with a very simple combination of a 90° Lorentzian, which we naturally associate with intrinsic pinning (noting that stacking faults can also commonly contribute also to this component at higher temperatures), and a broad (actually fully isotropic) Lorentzian, which we associate with pinning by point-like defects and nanoparticles. At 50 K, 5 T the isotropic component is required to become slightly anisotropic to cover a broad *c*-axis (0°) peak, while the inclusion of a broad bifurcated Gaussian also centred at 0° improves the fit. This broad Gaussian component is even more prominent at other conditions—see, for example, 65 K, 8 T in figure 2 and [40].—justifying the usage of this form here. We tentatively associate this minor Gaussian component with grain boundaries and twin planes on the basis that no other obvious *c*-axis oriented defects are apparent in these samples.

For the irradiated samples, these same components are used with the addition of a significant *c*-axis (0°) Lorentzian to fit the new peak resulting from the columnar defects. All components in these fits have been constrained at either 0° or 90° with a single common angular offset in each case to allow for experimental offsets. Further, for 50 K fits, the Γ parameter of the bifurcated Gaussian and the *c*-axis Lorentzian have been fixed to reduce the number of free parameters, with negligible impact on the quality or interpretation of fits. The I_0 and Γ parameters of all components are plotted in figure 6.

The changes brought about by irradiation are quantitatively quite different at 20 K and 50 K. In both cases, a Lorentzian peak centred at 0° appears, corresponding to extra pinning by the columnar defects. This new peak initially grows with irradiation fluence until it reaches the optimal fluence between 4×10^{11} cm^{-2} and 6×10^{11} cm^{-2}. Beyond that fluence it diminishes along with the other components. This peak is relatively more prominent at 50 K than at 20 K, but that is not to say that the extra pinning is stronger. At 20 K, a significant part of the weight from the 0° peak is transferred to both the isotropic component and the 90° peak (by way of broadening), giving a lift in I_c over almost the entire angular range. Only within a couple of degrees of 90° does the irradiation reduce I_c, and this is a result of the broadening of the 90° peak. At 50 K, on the other hand, the extra pinning is concentrated in the 0° peak making this a much more prominent feature, while I_c in the vicinity of the 90° peak remains similar to or less than the unirradiated sample.

With respect to the 90° (*ab* peak) Lorentzian, the peak value of this component generally decreases with increasing density of columnar defects. This is the behaviour commonly observed previously [34, 35]; the additional columnar defects are orthogonal to the vortices so tend to diminish rather than enhance pinning.

It is also apparent that at 20 K this *ab* peak broadens significantly following irradiation, whereas at 50 K it does not. We summarise this in figure 7 where the Γ peak-shape parameter of this component is replotted as a function of irradiation fluence for these two temperatures. For the 20 K peak, this parameter increases monotonically by over a factor of 3, whereas for the 50 K peak (which is sharper to begin with) it does not change appreciably. This broadening illustrates the greater propensity for staircase vortices to be pinned by the orthogonal extended defects—intrinsic planar pins and irradiation-induced columnar pins—at 20 K but not at 50 K.

By inspecting figure 2, it is clear that this distinction between behaviours at 20 K and 50 K extends to the full parameter space covered in our experiments. We speculate that the increasing importance of isotropic pinning by point defects (such as single oxygen vacancies) at lower temperatures plays a role in pinning staircase vortices and therefore broadening the 0° and 90° Lorentzian peaks, and it is clearly an interaction between the three types of defect—planar intrinsic pins, point-like defects and columnar defects—that induces the peak broadening. We note, for example, that in proton irradiated material, while the isotropic pinning is enhanced at 20 K by a similar amount as here, the 90° peak does not broaden appreciably [42].

The net effect is that pinning by the discontinuous columnar defects introduced by 100 MeV Ag ion irradiation produces

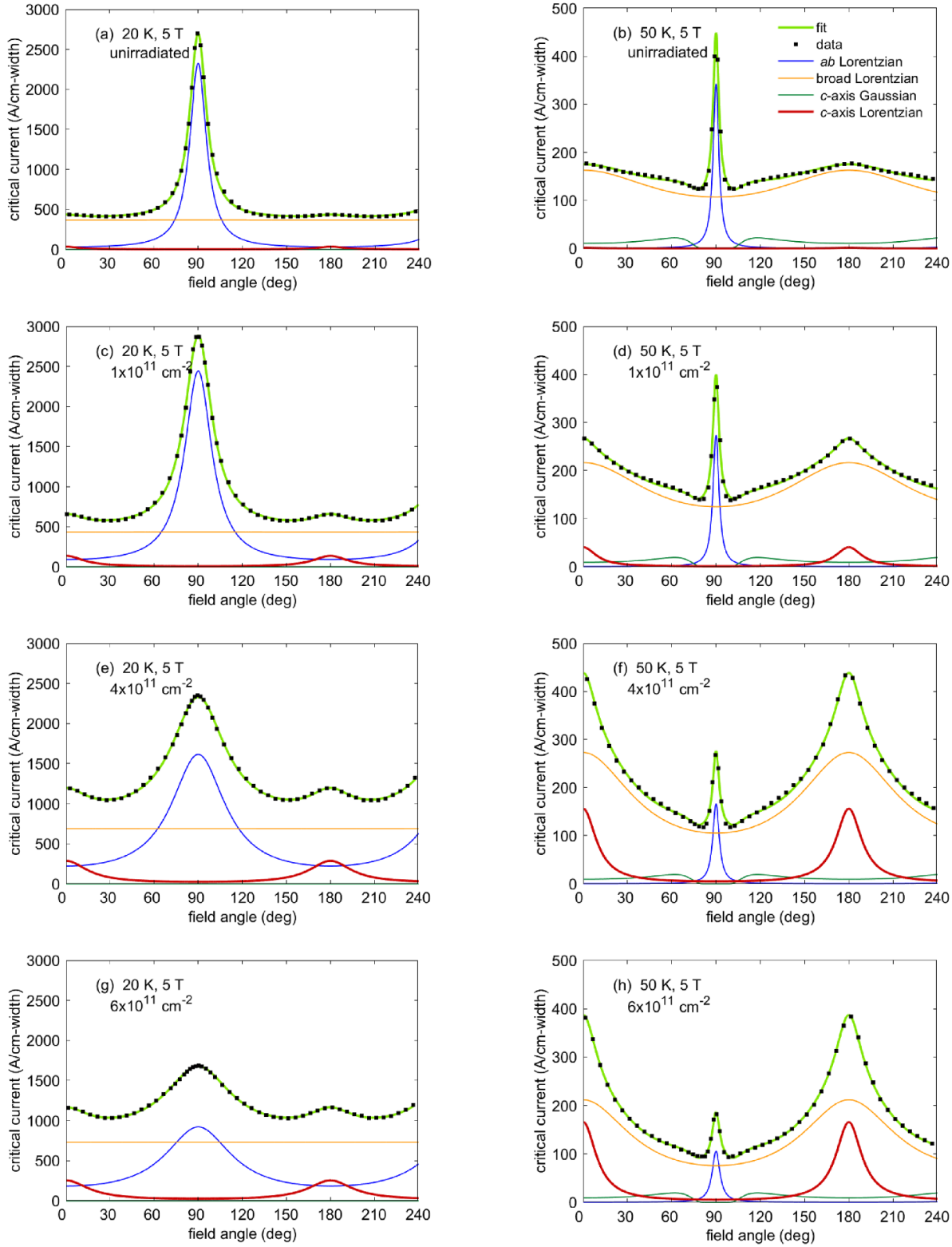

Figure 5. Decomposition of the angular dependence of I_c into maximum-entropy components at 20 K, 5 T (left column) and 50 K, 5 T (right column). The unirradiated sample (a) and (b) requires at 20 K a 90° Lorentzian and a broad Lorentzian and at 50 K an additional broad 0° Gaussian. The irradiated samples (c)–(h) require these same components and in addition a 0° Lorentzian. The legend in (b) applies to all plots.

a very strong enhancement only near 0° (for 0° irradiation incidence angle) at temperatures above 40 K, but also produces a significant *near-isotropic* enhancement below 40 K. Rather surprisingly, it is at the lowest temperatures that we observe the most useful enhancement of I_c through these columnar defects.

Table 1. Assignment of fit components to principal microstructural features.

Fit component	Microstructural feature	Mean direction
ab Lorentzian	Intrinsic pinning (and stacking faults)	90°
Broad Lorentzian	Point defects (oxygen vacancies) and nanoparticles	0°
c-axis Gaussian	Grain boundaries and twin planes	0°
c-axis Lorentzian	Columnar irradiation defects	0°

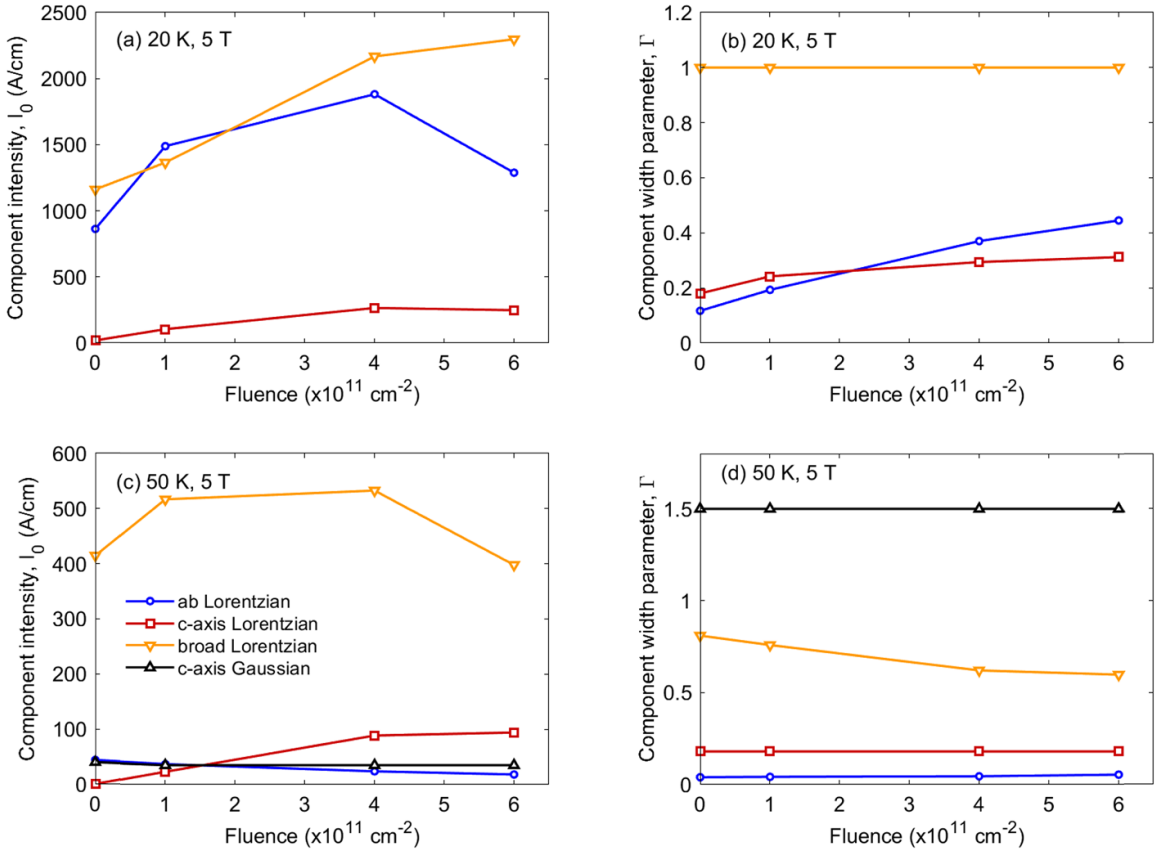

Figure 6. Variation with fluence of the peak-shape parameters I_0 and Γ for all of the components in the maximum entropy fits of figure 5. (a) I_0 at 20 K, 5 T, b) Γ at 20 K, 5 T, (c) I_0 at 50 K, 5 T and (d) Γ at 50 K, 5 T. The legend in (c) applies to all plots.

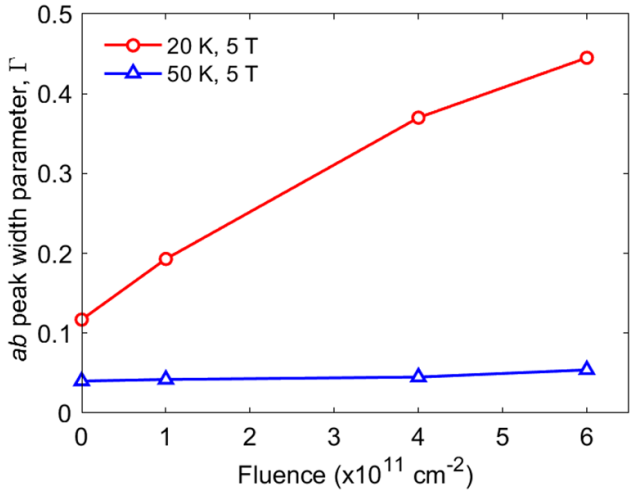

Figure 7. Variation with fluence of the peak-shape parameter Γ for the *ab*-plane (90°) peak arising from intrinsic pinning for measurements at 20 K and 50 K.

4. Conclusions

Irradiation with 100 MeV Ag ions produces discontinuous columnar defects in the REBCO layer of a coated conductor that significantly enhance the critical current when magnetic fields are applied parallel to the irradiation incidence angle. At temperatures above about 40 K this enhancement is limited to the angular range close to the incidence angle, and the critical current at other angles may be unaffected or even reduced. In particular, it is quite difficult to significantly increase the angular minimum I_c using normal-incidence irradiation. At lower temperatures though, the I_c enhancement broadens to the point that it merges with the in-plane intrinsic pinning peak, giving a nearly isotropic pinning response. In this regime, we have achieved a factor of 2.7 enhancement of the angular minimum I_c at 20 K, 3 T.

The near-isotropic I_c obtained at 20 K, 3 T is not an indication of reduced pinning by the planar and columnar defects, since the absolute I_c values are increased by a significant factor over the unirradiated sample, but rather is an illustration that pinning by combinations of defects can produce effects that are not simply additive. Similarly, the absence of a pinning peak does not necessarily demonstrate the absence of the corresponding extended defects. In these samples we suggest that a third population of pinning centres, namely point defects such as oxygen vacancies, that are present in all the samples including the unirradiated sample, become strong pins only at low temperatures and then combine with the planar and columnar features to create the near-isotropic I_c.

We have made use of the vortex-path model for quantifying peak broadening due to combinations of defects. This is made particularly clear through the possibility of precisely modifying the pinning landscape through ion irradiation.

Data availability statement

All data that support the findings of this study are included within the article (and any supplementary files).

Acknowledgments

This research has been supported by the Royal Society of New Zealand under Marsden Fund Grant VUW1805. We acknowledge access to the Heavy-Ion Accelerator Facility funded under the National Collaborative Research Infrastructure Strategy (NCRIS), Australia.

ORCID iDs

Nicholas M Strickland https://orcid.org/0000-0003-2784-1216
Stuart C Wimbush https://orcid.org/0000-0003-1636-643X
Arya Ambadiyil Soman https://orcid.org/0000-0001-6604-1196
Nicholas J Long https://orcid.org/0000-0003-2412-0683
Martin W Rupich https://orcid.org/0000-0002-2603-7763
Ruth Knibbe https://orcid.org/0000-0002-9931-7520
Ming Li https://orcid.org/0000-0002-4214-6556
Christian Notthoff https://orcid.org/0000-0002-6953-7207
Patrick Kluth https://orcid.org/0000-0002-1806-2432

References

[1] MacManus-Driscoll J L and Wimbush S C 2021 Processing and application of high-temperature superconducting coated conductors *Nat. Rev. Mater* **6** 587
[2] MacManus-Driscoll J L, Foltyn S R, Jia Q X, Wang H, Serquis A, Civale L, Maiorov B, Hawley M E, Maley M P and Peterson D E 2004 Strongly enhanced current densities in superconducting coated conductors of $YBa_2Cu_3O_{7-x}$ + $BaZrO_3$ *Nat. Mater.* **3** 439
[3] Selvamanickam V *et al* 2010 Enhanced and uniform in-field performance in long (Gd, Y)–Ba–Cu–O tapes with zirconium doping fabricated by metal–organic chemical vapor deposition *Supercond. Sci. Technol.* **23** 014014
[4] Mele P, Matsumoto K, Horide T, Ichinose A, Mukaida M, Yoshida Y, Horii S and Kita R 2008 Ultra-high flux pinning properties of $BaMO_3$-doped $YBa_2Cu_3O_{7-x}$ thin films (M = Zr, Sn) *Supercond. Sci. Technol.* **21** 032002
[5] Awaji S, Namba M, Watanabe K, Miura M, Yoshizumi M, Izumi T and Shiohara Y 2010 Flux pinning properties of TFA-MOD (Y,Gd)$Ba_2Cu_3O_x$ tapes with $BaZrO_3$ nanoparticles *Supercond. Sci. Technol.* **23** 014006
[6] Hänisch J, Cai C, Stehr V, Hühne R, Lyubina J, Nenkov K, Fuchs G, Schultz L and Holzapfel B 2006 Formation and pinning properties of growth-controlled nanoscale precipitates in $YBa_2Cu_3O_{7-\delta}$/transition metal quasi-multilayers *Supercond. Sci. Technol.* **19** 534
[7] Civale L *et al* 2004 Influence of crystalline texture on vortex pinning near the ab-plane in $YBa_2Cu_3O_7$ thin films and coated conductors *Physica* C **412** 976
[8] Specht E D, Goyal A, Li J, Martin P M, Li X and Rupich M W 2006 Stacking faults in $YBa_2Cu_3O_{7-x}$: measurement using x-ray diffraction and effects on critical current *Appl. Phys. Lett.* **89** 162510
[9] Talantsev E F, Strickland N M, Wimbush S C, Storey J G, Tallon J L and Long N J 2014 Hole doping dependence of critical current density in $YBa_2Cu_3O_{7-\delta}$ conductors *Appl. Phys. Lett.* **104** 242601
[10] Puichaud A-H, Wimbush S C and Knibbe R 2017 Enhanced low-temperature critical current by reduction of stacking faults in REBCO coated conductors *Supercond. Sci. Technol.* **30** 074005
[11] Long N, Strickland N, Chapman B, Ross N, Xia J, Li X, Zhang W, Kodenkandath T, Huang Y and Rupich M 2005 Enhanced in-field critical currents of YBCO second-generation (2G) wire by Dy additions *Supercond. Sci. Technol.* **18** S405
[12] Haugan T, Barnes P N, Wheeler R, Meisenkothen F and Sumption M 2004 Addition of nanoparticle dispersions to enhance flux pinning of the $YBa_2Cu_3O_{7-x}$ superconductor *Nature* **430** 867
[13] Gutierrez J *et al* 2007 Strong isotropic flux pinning in solution-derived $YBa_2Cu_3O_{7-x}$ nanocomposite superconductor films *Nat. Mater.* **6** 367
[14] Strickland N M, Long N J, Talantsev E F, Hoefakker P, Xia J, Rupich M W, Kodenkandath T, Zhang W, Li X and Huang Y 2008 Enhanced flux pinning by $BaZrO_3$ nanoparticles in metal-organic deposited YBCO second-generation HTS wire *Physica* C **468** 183
[15] Miura M, Maiorov B, Baily S A, Haberkorn N, Willis J O, Marken K, Izumi T, Shiohara Y and Civale L 2011 Mixed pinning landscape in nanoparticle-introduced

YGdBa$_2$Cu$_3$Oy films grown by metal organic deposition *Phys. Rev.* B **83** 184519
[16] Awaji S, Namba M, Watanabe K, Miura M, Yoshizumi M, Izumi T and Shiohara Y 2010 Flux pinning properties of TFA-MOD (Y,Gd)Ba$_2$Cu$_3$O*x* tapes with BaZrO$_3$ nanopartcles *Supercond. Sci. Technol.* **33** 014006
[17] Xu A, Jaroszynski J, Kametani F and Larbalestier D 2015 Broad temperature range study of J_c and H_{irr} anisotropy in YBa$_2$Cu$_3$O$_x$ thin films containing either Y$_2$O$_3$ nanoparticles or stacking faults *Appl. Phys. Lett.* **106** 052603
[18] Strickland N M, Long N J, Talantsev E F, Hoefakker P, Xia J A, Rupich M W, Zhang W, Li X, Kodenkandath T and Huang Y 2008 Nanoparticle additions for enhanced flux pinning in YBCO HTS films *Curr. Appl. Phys.* **8** 372
[19] Maiorov B, Baily B A, Zhou H, Ugurlu O, Kennison J A, Dowden P C, Holesinger T G, Foltyn S R and Civale L 2009 Synergetic combination of different types of defect to optimize pinning landscape using BaZrO$_3$-doped YBa$_2$Cu$_3$O$_7$ *Nat. Mater.* **8** 398
[20] Civale L, Marwick A D, Worthington T K, Kirk M A, Thompson J R, Krusin-Elbaum L, Sun Y, Clem J R and Holtzberg F 1991 Vortex confinement by columnar defects in YBa$_2$Cu$_3$O$_7$ crystals: enhanced pinning at high fields and temperatures *Phys. Rev. Lett.* **67** 648
[21] Civale L 1997 Vortex pinning and creep in high-temperature superconductors with columnar defects *Supercond. Sci. Technol.* **10** 184519
[22] Holzapfel B, Kreiselmeyer G, Kraus M, Saemann-Ischenko G, Bouffard S, Klaumunzer S and Schultz L 1993 Angle-desolved critical transport-current density of YBa$_2$Cu$_3$O$_{7-\delta}$ thin films and YBa$_2$Cu$_3$O$_{7-\delta}$/ PrBa$_2$Cu$_3$O$_{7-\delta}$ superlattices containing columnar defects of various orientations *Phys. Rev.* B **48** 600
[23] Civale L, Marwick A D, McElfresh M W, Worthington T K, Malozemoff A P, Holtzberg F, Thompson J R and Kirk M A 1990 Defect independence of the irreversibility line in proton-irradiated Y-Ba-Cu-O crystals *Phys. Rev. Lett.* **65** 1164
[24] Eley S, Leroux M, Rupich M W, Miller D J, Sheng H, Niraula P M, Kayani A, Welp U, Kwok W-K and Civale L 2017 Decoupling and tuning competing effects of different types of defects on flux creep in irradiated YBCO coated conductors *Supercond. Sci. Technol.* **30** 015010
[25] Leroux M *et al* 2015 Rapid doubling of the critical current of YBa$_2$Cu$_3$O$_{7-\delta}$ coated conductors for viable high-speed industrial processing *Appl. Phys. Lett.* **107** 192601
[26] Kihlstrom K J *et al* 2021 Large enhancement of the in-field critical current density of YBCO coated conductors due to composite pinning landscape *Supercond. Sci. Technol.* **34** 015011
[27] Sueyoshi T 2021 Modification of critical current density anisotropy in high-Tc superconductors by using heavy-ion irradiations *Quantum Beam Sci.* **5** 16
[28] Sueyoshi T, Kotaki T, Furuki Y, Uraguchi Y, Kai T, Fujiyoshi T, Shimada Y, Yasuda K and Ishikawa N 2015 Influence of discontinuous columnar defects on flux pinning properties in GdBCO coated conductors *IEEE Trans. Appl. Supercond.* **25** 6603004
[29] Sueyoshi T, Sogo T, Nishimura T, Fujiyoshi T, Mitsugi T, Ikegami T, Awaji S, Watanabe K, Ichinose A and Ishikawa N 2016 Angular behaviour of critical current density in YBa$_2$Cu$_3$O$_y$ thin films with crossed columnar defects *Supercond. Sci. Technol.* **29** 065023
[30] Rupich M W *et al* 2016 Engineered pinning landscapes for enhanced 2G coil wire *IEEE Trans. Appl. Supercond.* **26** 6601904
[31] Jia Y *et al* 2013 Doubling the critical current density of high temperature superconducting coated conductors through proton irradiation *Appl. Phys. Lett.* **103** 122601
[32] Suvorova E I, Degtyarenko P N, Karateev I A, Ovcharov A V, Vasiliev A L, Skuratov V A and Buffat P A 2019 Energy dependent structure of Xe ion tracks in YBCO and the effect on the superconductive properties in magnetic fields *J. Appl. Phys.* **126** 145106
[33] Weinstein R, Gandini A, Sawh R, Parks D and Mayes B 2003 Improved pinning regime by energetic ions using reduction of pinning potential *Physica* C **387** 391
[34] Strickland N M, Talantsev E F, Long N J, Xia J A, Searle S D, Kennedy J, Markwitz A, Rupich M W, Li X and Sathyamurthy S 2009 Flux pinning by discontinuous columnar defects in 74 MeV Ag-irradiated YBa$_2$Cu$_3$O$_7$ coated conductors *Physica* C **469** 2060
[35] Strickland N, Wimbush S, Kennedy J, Ridgway M, Talantsev E and Long N 2015 Effective low-temperature flux pinning by Au ion irradiation in HTS coated conductors *IEEE Trans. Appl. Supercond.* **25** 6939646
[36] Strickland N M, Wimbush S C, Soman A A, Kluth P, Notthoff C, Knibbe R, Li M and Rupich M W 2022 Isotropic and anisotropic flux pinning induced by heavy-ion irradiation *IEEE Trans. Appl. Supercond.* **32** 8000505
[37] Rupich M W, Li X, Sathyamurthy S, Thieme C L H, Demoranville K, Gannon J and Fleshler S 2013Second generation wire development at AMSC *IEEE Trans. Appl. Supercond.* **23** 6601205
[38] Strickland N M, Wimbush S C, Pantoja A, Pooke D M, Fee M, Chamritskii V, Hartwig Z, Cheng J, Garberg S and Sorbom B 2021 Extended-performance "SuperCurrent" cryogen-free transport critical-current measurement system *IEEE Trans. Appl. Supercond.* **31** 9000305
[39] Soman A A, Wimbush S C, Rupich M W, Notthoff C, Kluth P, Knibbe R, Li M and Strickland N M 2022 The role of stacking faults in the enhancement of the *a-b* plane peak in silver ion-irradiated commercial MOD REBCO wires *IEEE Trans. Appl. Supercond.* **32** 8000405
[40] Strickland N M, Soman A A, Rupich M W and Wimbush S C 2022 Onset temperature of intrinsic pinning in a REBCO coated conductor from critical current anisotropy *Superconductivity* **4** 100025
[41] Strickland N M and Wimbush S C 2017 The magnetic field dependence of critical current: what we really need to know *IEEE Trans. Appl. Supercond.* **27** 8000505
[42] Soman A A, Wimbush S C, Long N J, Rupich M W, Leveneur J, Kennedy J and Strickland N M 2023 unpublished
[43] Long N J, Strickland N M and Talantsev E F 2007 Modeling of vortex paths in HTS *IEEE Trans. Appl. Supercond.* **17** 3684
[44] Wimbush S C and Long N J 2012 The interpretation of the field angle dependence of the critical current in defect-engineered superconductors *New J. Phys.* **14** 083017
[45] Long N J 2008 Model for the angular dependence of critical currents in technical superconductors *Supercond. Sci. Technol.* **21** 025007
[46] Long N J 2017 Critical current anisotropy in relation to the pinning landscape *Vortices and Nanostructured Superconductors* vol 261, ed A Crisan *(Cham: Springer Series in Materials Science)* (https://doi.org/10.1007/978-3-319-59355-5_4)